ADVANCED MATERIALS INTERFACES
www.advmatinterfaces.de

Deposition Dependent Ion Transport in Doped Conjugated Polymer Films: Insights for Creating High-Performance Electrochemical Devices

*Lushuai Zhang and Trisha L. Andrew**

Charge conduction and redox events in films of doped conjugated polymers are necessarily accompanied by counterion transport. However, insights into how deposition conditions affect ion transport in a structurally diverse set of doped conjugated polymer films and across a polymer/electrolyte interface have not been gathered. Here, cyclic voltammetry and electrogravimetry measurements are used to probe solvent and ion transport across a doped conjugated polymer/electrolyte interface. A representative polymer, *p*-doped poly(3,4-ethlyenedioxythiophene) (PEDOT), obtained using two different deposition methods, vapor phase polymerization (VPP) and oxidative chemical vapor deposition (oCVD), is studied. PEDOT films obtained via VPP and oCVD display dissimilar morphologies at the micro- and nanometer length scales, resulting in significantly differing swelling behavior, mass trapping, and ion transport upon exposure to a periodic applied potential. PEDOT films obtained using oCVD display notable permselectivity and near-ideal mass transport during repeated doping/dedoping cycles in various electrolytes, indicating that these films are robust electroactive materials. This study underlines the extent to which film deposition conditions affect ion transport across polymer/electrolyte interfaces and provides insights into optimal film forming conditions for high-performance supercapacitors and electrochemical transistors.

1. Introduction

Doped conjugated polymers have resurged as enabling components in a variety of nascent technologies, including flexible integrated circuits,[1,2] hybrid supercapacitors,[3–7] tissue-compatible biosensors and medical implants,[8–15] and neural network simulants.[16] These soft electronic materials are also longstanding, reliable choices for conductive channels in ion sensors,[13–15] color modulators in electrochromic devices,[17,18] and actuating materials in artificial muscles.[19]

Charge conduction and redox events in films of doped conjugated polymers are necessarily accompanied by counterion transport.[20] When interfaced with an electrolyte, redox events in conjugated polymer films are also accompanied by film swelling or deswelling due to ion and/or solvent diffusion into or out of the films, respectively. The response times and fatigue resistances of devices that subject electroactive films to periodic cycles of oxidation/reduction are, thus, crucially determined by solvent intercalation and/or ion transport across an interface and mass trapping within the conductive polymer layer.[21,22]

Innovations in film deposition routines[23,24] and doping protocols have resulted in huge leaps in the electronic conductivities of doped conjugated polymer films, even reaching the metallic regime in the composite material poly(3,4-ethylenedioxythiophene)-*co*-poly(styrene sulfonic acid) (PEDOT:PSS).[25–27] However, correlated insights into how these processing conditions affect redox-associated swelling behavior and ion transport in doped conjugated polymer films (other than PEDOT:PSS) is lacking. This knowledge is integral for optimizing the performance of polymer-based hybrid supercapacitors and enabling accurate data interpretation from electrochemical transistors, among other applications.[28,29]

In this work, we use simultaneous electrochemical and electrogravimetric measurements[30–34] to probe, in situ, the swelling behavior, permselectivity and electrochemical cycling stabilities[35–37] of a model material, *p*-doped PEDOT, in selected electrolytes. In particular, we pay attention to the effects of deposition method on the electrochemical and electrogravimetric properties of resulting films. Our efforts reveal that PEDOT films obtained using oxidative chemical vapor deposition display notable permselectivity and near-ideal redox-associated mass transport during repeated doping/dedoping cycles.

2. Results and Discussion

Solid-state morphology is known to significantly influence the optical and electronic properties of soft electronic materials. Here, we sought to systematically investigate the electrochemical and electrogravimetric properties of films of a

Dr. L. Zhang, Prof. T. L. Andrew
Departments of Chemistry and Chemical Engineering
University of Massachusetts Amherst
Amherst, MA 01003, USA
E-mail: tandrew@umass.edu

The ORCID identification number(s) for the author(s) of this article can be found under https://doi.org/10.1002/admi.201700873.

DOI: 10.1002/admi.201700873

 © 2017 WILEY-VCH Verlag GmbH & Co. KGaA, Weinheim

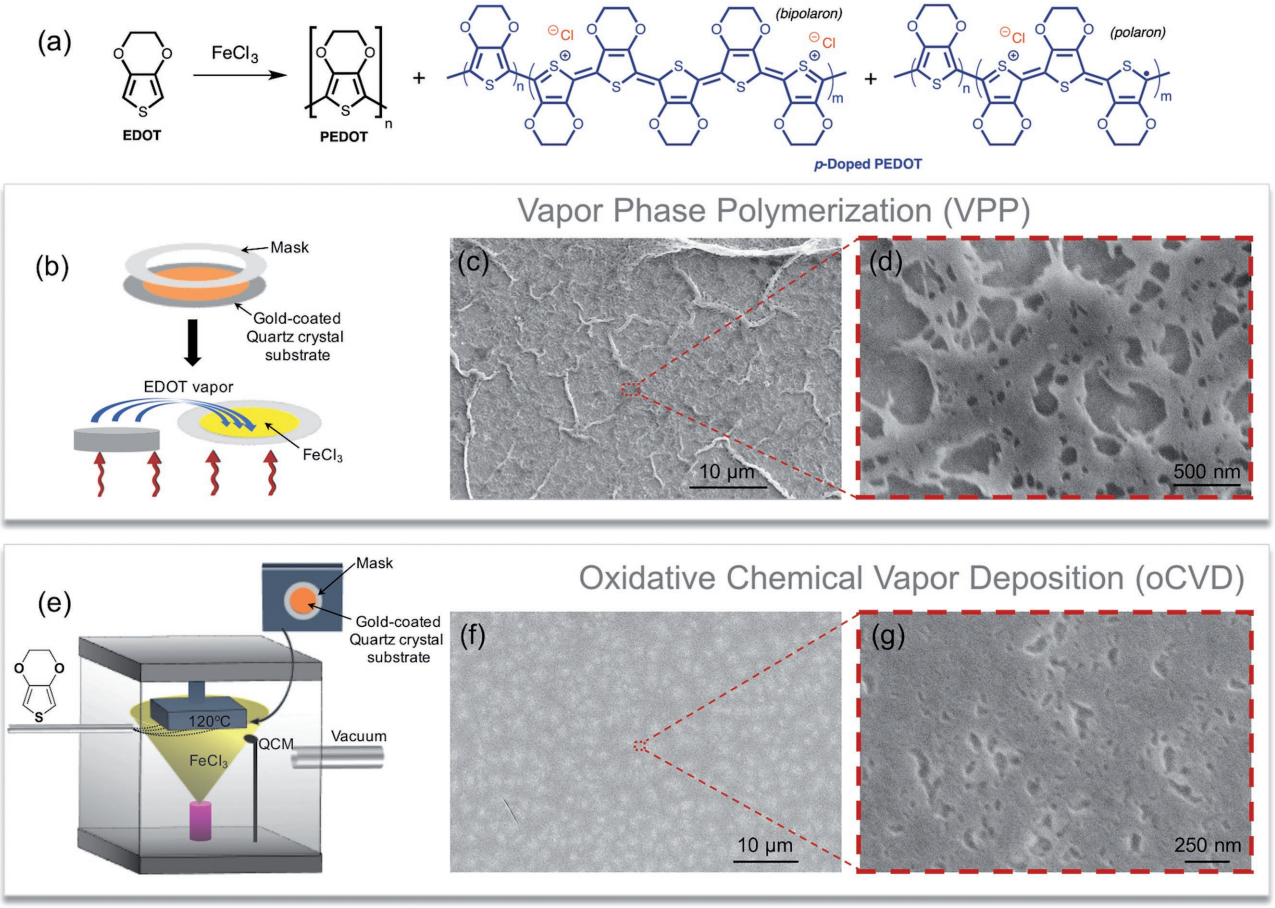

Figure 1. a) Polymerization reaction underlying the vapor deposition methods studied herein. Cartoon illustrations of b) VPP and e) oCVD deposition methods. SEM images of 100 nm thick PEDOT film prepared by VPP c) and d), showing a rough surface over a large length scale c) and widely distributed pore sizes d). SEM images of 80 nm thick PEDOT film prepared by oCVD f) and g), showing a uniform and smooth film over a large length scale f) and nanometer-scale pores with a narrow size distribution g).

model conducting polymer, *p*-doped PEDOT, created using two different vapor deposition methods that are widely used in contemporary research efforts (**Figure 1**).

Vapor-phase polymerization (VPP) is an approach where a substrate is first coated or impregnated with a solid film of an oxidant and then exposed to vapors of selected volatile monomers in a closed environment at elevated temperatures. The oxidant creates radical cations of the monomer on the substrate surface, which then dimerize and/or react with growing oligomer chains to form conjugated oligomers and polymers via a step-growth mechanism. Currently, VPP is one of the most commonly used methods with which to create electronic coatings on insulating substrates, such as plastics and textiles, for wearable and flexible devices.[38,39]

Oxidative chemical vapor deposition (oCVD) is a comparatively nascent approach[40–42] and involves introducing *both* the oxidant and a monomer as *vapors* into a low-pressure reaction chamber containing a temperature-controlled substrate stage. oCVD affords real-time control over mass transport and the effective path length of the reactant vapors, yielding uniform and conformal films on rough and textured surfaces.[40,41]

The chemical structure of the polymer repeat unit and the counterion identity were the same for polymer films we obtained using either oCVD or VPP, since iron (III) chloride was used as a common oxidant. Further, since we did not employ reaction additives or subject our films to any post-deposition treatments, the conductivities of the films obtained via VPP and oCVD were similar. However, the morphologies of PEDOT films obtained using oCVD versus VPP were significantly different (Figure 1). oCVD produced smooth (on the micrometer scale) and uniform films of consistent thickness across different deposition batches. On the nanometer scale, multiple pores could be observed, which we posited could facilitate ion and solvent diffusion. In stark contrast, VPP created films with noticeable roughness and creasing on the micrometer scale. Further, a wide distribution of pore sizes was also observed, ranging from few tens of micrometers to tens of nanometers wide; the distribution of pore sizes was also found to vary batch-to-batch.

Next, the electrochemical properties of the films obtained via oCVD or VPP were characterized using an electrochemical quartz crystal microbalance (eQCM), which performs simultaneous cyclic voltammetry-electrogravimetry (CV-EG) experiments. An eQCM measures changes in the mass of an electroactive material with varying applied potential. Compared to device characterization data, eQCM measurements

 © 2017 WILEY-VCH Verlag GmbH & Co. KGaA, Weinheim

offer systematic, quantitative and richly detailed information on redox-associated solvent swelling, ion intercalation, and mass trapping in electroactive films. To wit, eQCM measurements provided a groundbreaking understanding of anomalous capacitance and charging mechanisms in porous carbon-based charge storage devices.[30–34] Extensive eQCM characterization of electrodeposited PEDOT films also lead to the identification and optimization of robust and biocompatible sensing elements.[35–37]

In a typical scan, a linearly increasing potential is first applied to oxidize (dope) a conjugated polymer film and the potential is then linearly decreased to the starting value to dedope the polymer. Doping is accompanied by film swelling due to the migration of counterions (anions) and solvent into the oxidized film. In an ideal material, complete dedoping can be achieved without the need for an applied overpotential and any ions and solvent molecules will completely migrate out of the film upon dedoping. However, in practice, conjugated polymer films are nonideal, and solvent, ions, and charge remain trapped in the film after dedoping. Such mass and charge trapping leads to electrochemical fatigue (i.e., hysteresis and/or steadily increasing onset potentials) and reduced performance in electrochemical devices,[3,4,20] such as supercapacitors[43,44] and electrochemical transistors.

Figure 2 displays the gravimetric characteristics of PEDOT films obtained via oCVD or VPP during three sequential doping/dedoping cycles. The gray lines reveal the applied potential versus time, and the colored lines show the Δmass vs time response of the films in various electrolytes. Aqueous NaF, NaCl, and sodium tosylate (NaOTs) were used as electrolytes to investigate anion size effects on gravimetric response, and NaCl in 1:1 H_2O:acetonitrile (ACN) was used to investigate different solvent swelling effects.

The Δmass versus time responses for the PEDOT films obtained via oCVD were identical for repeated doping/dedoping cycles in all investigated electrolytes. Minimal differences were observed for data recorded in aqueous versus mixed acetonitrile/water electrolytes, suggesting that solvent swelling did not cause irreversible and, possibly, detrimental chain rearrangement[21,22] in the PEDOT-oCVD film. More importantly, the starting and ending Δmass values for each cycle were nearly identical for all investigated electrolytes, revealing that any ion or solvent that enters the PEDOT film upon doping was efficiently transported out of the film upon dedoping.

In contrast, the Δmass versus time curves for the PEDOT film obtained via VPP displayed persistent and additive mass increases at the end of each cycle, meaning that intercalated ions and/or solvent remained trapped in the film after dedoping. Such mass trapping is particularly evident in NaCl electrolytes, even at the end of the second consecutive doping/dedoping cycle. We posit that bulky tosylate (TsO^-) anions do not permeate into the polymer film as thoroughly as the smaller chloride anions and, therefore, easily migrate out of the films upon dedoping. These observations indicate that electrochemical devices containing PEDOT films created via VPP, such as hybrid supercapacitors and electrochemical transistors, should display poor electrochemical fatigue resistance and reduced performance over time.

Figure 2 only displays the electrogravimetric response for PEDOT films over three consecutive redox cycles because

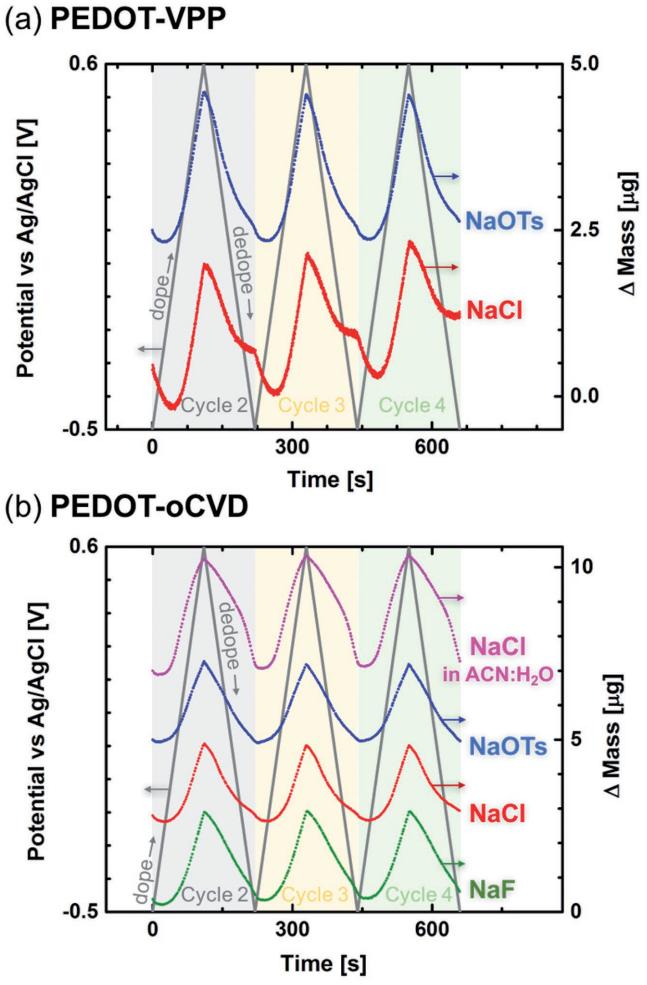

Figure 2. a) Electrogravimetry traces recorded during the second, third, and fourth consecutive doping/dedoping cycles in various electrolytes for PEDOT films obtained via a) VPP or b) oCVD. The gray lines show the applied potential versus time. The colored lines show the resulting mass change versus time. Scan rates were 10 mV s^{-1} for all measurements.

notable mass trapping was evident in the films obtained via VPP even after the end of the second cycle. In comparison, films obtained via oCVD did not suffer from such mass trapping after a small number of redox cycles, even though there exist only subtle differences between the two vapor deposition procedures. Therefore, the results displayed in Figure 2 highlight the unexpected degree to which deposition procedure can influence electrochemical robustness.

A more detailed picture of the composition of mass flux accompanying redox events can be gathered by plotting the Δmass response versus Δcharge. Observed mass changes can be correlated to the amount of charge passed through the PEDOT-coated crystal sensor using Faraday's law[33]

$$m = \frac{Q \cdot M_w}{n \cdot F} \tag{1}$$

where Q is the charge passed through the electrode in Coulombs (obtained by integrating the cyclic voltammogram), M_w

© 2017 WILEY-VCH Verlag GmbH & Co. KGaA, Weinheim

is the molecular weight of the ion, F is the Faraday constant (96 485 C mol^{-1}), and n is the valence charge value of the ion. Rewriting Faraday's law (Equation (1)) leads to Equation (2)

$$\frac{\Delta m}{\Delta Q} = \frac{M_{\mathrm{w}}^{\mathrm{app}}}{n \cdot F} \tag{2}$$

Therefore, the apparent molecular weight $\left(M_{\mathrm{w}}^{\mathrm{app}}\right)$ of the ions that interact with polymer film can be calculated from the slope of Δm versus ΔQ curve.

The calculated Δmass versus Δcharge plots in aqueous NaF, NaCl, and sodium tosylate electrolytes for PEDOT films created using either VPP or oCVD are shown in **Figure 3**. The insets show the as-recorded cyclic voltammograms (CVs) and correlated electrogravimetry curves. All scans were started after initial mass equilibrium was reached (see Figure S1, Supporting Information, and the Experimental Section). Each measurement included a forward scan (from –0.5 to 0.6 V) and a reverse scan (from 0.6 to –0.5 V), corresponding to doping and dedoping, respectively. The arrows indicate the direction of applied potential for each scan. As shown in **Figure 4**a,b, a small decrease in mass was first manifested at the beginning of the forward scan, followed by a region of steep mass increase, then a saturation region. During the reverse scan, mass first monotonically then gradually decreased back to zero with decreasing potential.

To systematically interpret the data shown in Figure 3, we divided the forward scan into three domains (FW I, FW II, and FW III) and the reverse scan into two domains (RV I and RV II) based on the varying slopes of the Δmass versus Δcharge curves. The orange and green circles in Figure 3 denote the boundary between FW I and FW II domains and that between RV I and RV II domains, respectively. Thorough illustrations of domain designations for all measured data are shown in Figure S2 in the Supporting Information. The calculated $\left(M_{\mathrm{w}}^{\mathrm{app}}\right)$ in different domains are summarized in **Table 1**.

Informed by detailed discussions in previous CV-EG reports,[35–37] we ascribed the following phenomena to each identified region:

1. *FW I*. In the region between –0.5 and –0.25 V of the forward scan, field-driven solvent expulsion out of the PEDOT film should lead to a small mass decrease.
2. *FW II*. PEDOT is oxidized (doped) in the potential region between –0.25 and 0.6 V, which should lead to a linear mass increase due to anion flux into the films. Anions should be pulled into the oxidized PEDOT films by both the electrostatic attraction of anions to the positively charged polymer and field-driven anion migration toward the working electrode.
3. *FW III*. The degree of oxidation of PEDOT films should saturate at high, positive potentials and most of the free volume in the films is also likely filled with large, solvated anions. Therefore, any observed mass gains with potential > 0.6 V are expected to be small compared to the FW II region.
4. *RV I*. PEDOT is dedoped during the reverse scan, primarily in the region between 0.6 and –0.25 V. Therefore, field-driven solvent diffusion and anion migration out of the PEDOT film to the counter electrode should lead to a linear mass decrease in this domain.
5. *RV II*. Dedoping-associated mass loss due to anion and solvent expulsion should, ideally, continue in the small potential window from –0.25 to –0.5 V. However, if anions remain trapped, then cation migration into the film from the electrolyte will accompany dedoping to maintain charge balance. A mixture of cation diffusion into the film and anion expulsion out of the film can coexist in this potential region, leading to an overall lowered observed mass decrease compared to RV I.

We focused on comparing the apparent mass gains and mass losses in regions FW II and RV I, respectively, for differently deposited PEDOT films in various electrolytes, since these two regions were predicted to display linear Δmass responses versus Δcharge. As tabulated in Table 1, in a sodium chloride electrolyte, a larger mass gain in the FW II region was apparent compared to the mass loss recorded in the RV I region for the PEDOT film obtained by VPP. This quantification is consistent with the mass trapping revealed in Figure 2.

In a NaOTs electrolyte, the calculated values for apparent mass gain and mass loss were both smaller than the molecular mass of the tosylate ion (TsO^-, 171 g mol^{-1}). This discrepancy means that, for each unit of charge injected into the PEDOT film from the electrode interface, one correlated tosylate anion does not enter the film from the electrolyte interface to balance the charge in the film or vice versa. Due to the nonuniform film morphology and broad distribution of pore sizes in VPP PEDOT (Figure 1), it is likely that bulky tosylate anions do not thoroughly permeate into the film and, instead, get trapped within certain physical regions, leading to nonideal mass transport, both within the PEDOT film and at the polymer/electrolyte interface. Such trapping should create "charge islands" or areas of accumulated positive and negative charge throughout the film over time, which will lead to field screening, ion localization, and further-hampered mass transport with increasing redox cycles.

In contrast, PEDOT films created using oCVD displayed well-behaved, correlated anion motion with charge injection/expulsion, across all electrolytes studied herein. Further, the value of the calculated apparent mass lost per unit charge in the RV I region was approximately similar to that gained in region FW II, reaffirming the qualitatively reversible behavior revealed in Figure 2. The calculated apparent mass gain per unit charge in the FW II region for the oCVD PEDOT film could be clearly assigned to the migration of hydrated fluoride, chloride, or tosylate anions into the film. As expected, the degree of solvation (hydration) inversely scaled with the size of the anion.

Next, we sought to confirm that mass gains and losses in domains FW II and RV I were solely due to anion motion and, therefore, should be cation independent. To this end, CV-EG experiments were conducted in various aqueous alkali metal chloride electrolytes. The calculated Δmass versus Δcharge curves measured in LiCl, KCl, and CsCl are shown in Figure S3 in the Supporting Information. The calculated values of apparent mass gain in the FW II doping region and apparent mass loss in the RV I dedoping region are summarized in **Table 2**. Indeed, a dependence of the apparent mass gain/loss on the atomic mass of the cation was not evident. Instead, similar values of $\left(M_{\mathrm{w}}^{\mathrm{app}}\right)$ with slightly varying hydration values were

© 2017 WILEY-VCH Verlag GmbH & Co. KGaA, Weinheim

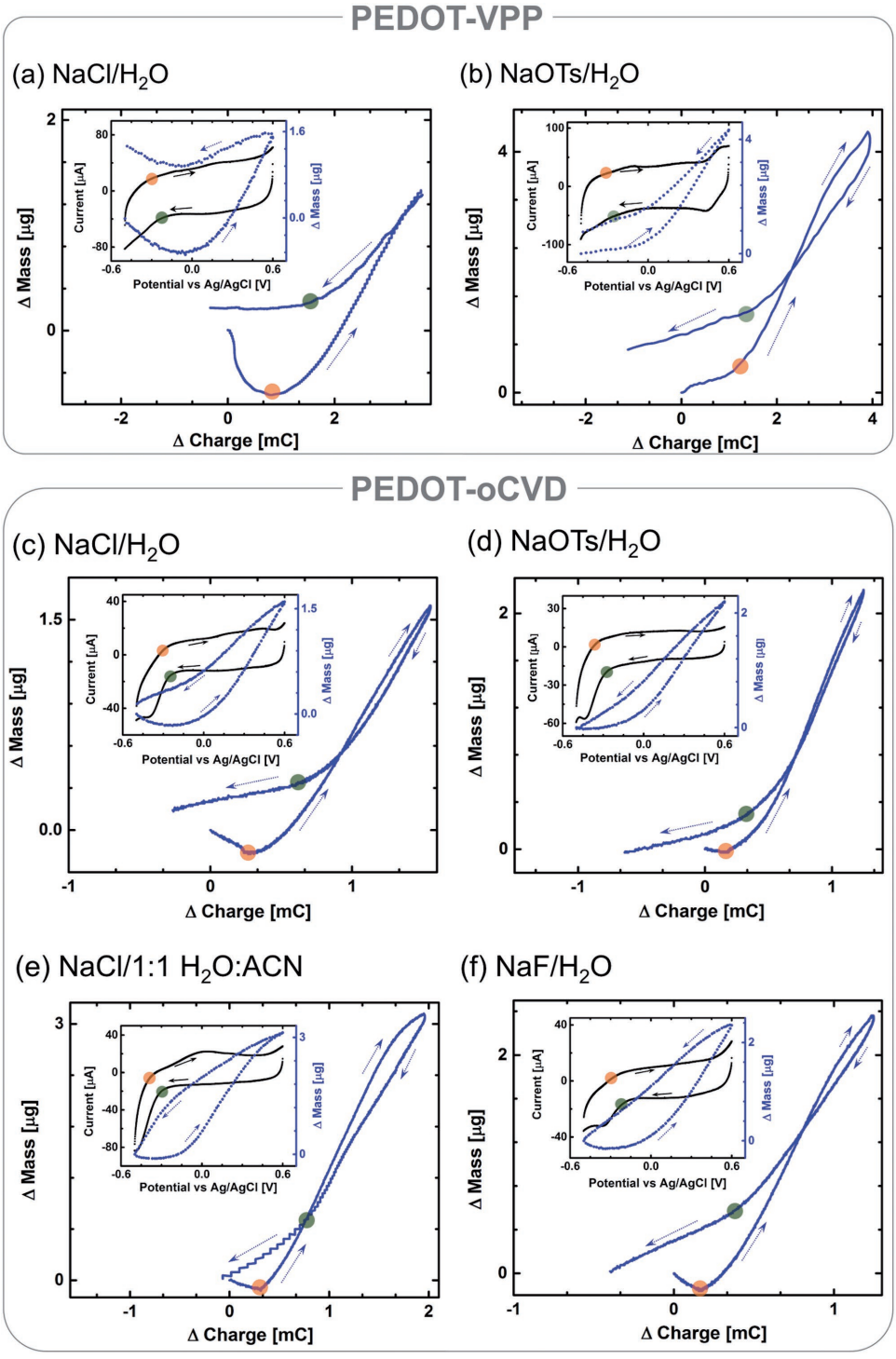

Figure 3. Calculated Δmass versus Δcharge plots for PEDOT films obtained via a,b) VPP or c–f) oCVD in various electrolytes. The arrows show the scan direction. The insets show the as-recorded voltammogram and gravimetry curves for each measurement. The orange and green dots indicate the onset of the FW II region and the end of the RV I region, respectively.

observed, confirming permselective anionic motion in PEDOT films created using oCVD.

Finally, we sought to investigate the electrogravimetric behavior of differently deposited PEDOT films when exposed to a representative bulky anion, tetraphenylborate.[45] As seen in Figure 4, cyclic voltammograms recorded in a sodium tetraphenylborate electrolyte for PEDOT films deposited via oCVD and VPP were significantly different than those recorded in previous electrolyte solutions (see Figure S4, Supporting Information, for a comparison). We hypothesized that a near absence

 © 2017 WILEY-VCH Verlag GmbH & Co. KGaA, Weinheim

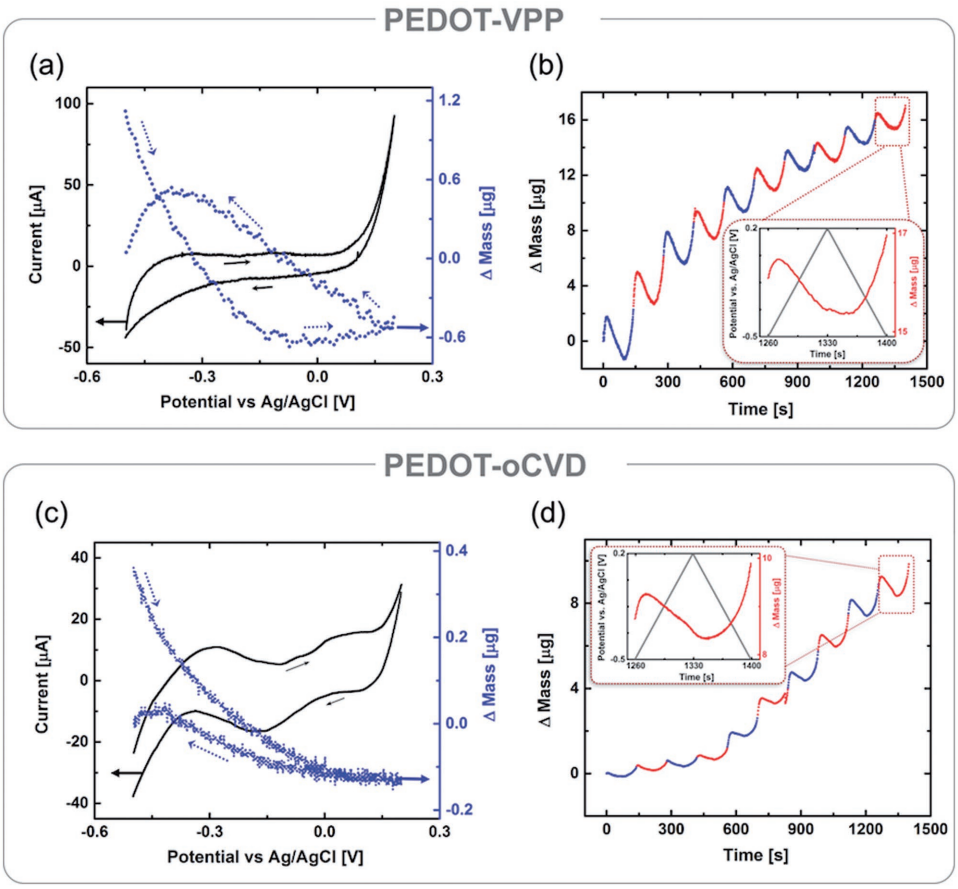

Figure 4. Electrochemical and electrogravimetric measurements of PEDOT films in aqueous sodium tetraphenylborate electrolyte. Potential dependent current and mass change recorded for PEDOT films obtained via a) VPP and c) oCVD. b,d) Electrogravimetric measurements versus time over ten consecutive doping/dedoping cycles for the two PEDOT films. The insets show the applied potential and correlated mass change for the tenth redox cycle.

of correlated anion entry into the film with charge injection created nonuniform areas of charge accumulation within the film, leading to charge screening, low overall recorded currents, and false peaks and valleys in the observed voltammograms. The recorded mass change versus time curves for each doping/dedoping cycle confirmed that redox events were not cleanly correlated with mass gain/loss, being surprisingly accompanied with mass loss during doping then mass gain during dedoping. The likely origins of these observations are that, during the forward scan, solvent migrated out of film and few tetraphenylborate anions were trapped in the films to serve as the counterions for the positively charged (doped) polymer. During the reverse scan, as positive charges disappeared from the polymer backbone, cations migrated into the film to compensate for the negative charge of the trapped tetraphenylborate anions. Such mixed cation and anion motion was supported by the small values for mass gain in the FW II region and mass loss in the RV I regions calculated for PEDOT films obtained by oCVD: 44 and 39 g mol^{-1}, respectively.

Overall, for electrolytes containing bulky anions, permselectivity seemed to break down for PEDOT films obtained via either VPP or oCVD. Also, both films displayed inefficient

Table 1. Apparent mass gain and loss during one doping/dedoping cycle for PEDOT films in various sodium electrolytes.

Deposition condition	Anion (molecular weight [g mol^{-1}])	Apparent mass gain in FW II [g mol^{-1}] (anion + n solvent)	Apparent mass loss in RV I [g mol^{-1}] (anion + n solvent)
VPP	Cl^- (35)	90 (n = 3.0)	57 (n = 1.2)
VPP	TsO^- (171)	156	139
oCVD	F^- (19)	290 (n = 15.0)	204 (n = 10.2)
oCVD	Cl^- (35)	167 (n = 7.3)	169 (n = 7.4)
oCVD	Cl^- in H_2O:ACN	240 (n = 7.0)	185 (n = 5.1)
oCVD	TsO^- (171)	267 (n = 5.3)	249 (n = 4.3)

© 2017 WILEY-VCH Verlag GmbH & Co. KGaA, Weinheim

Table 2. Apparent mass gain and loss during one doping/dedoping cycle for PEDOT-oCVD films in various alkali halide electrolytes.

	Apparent mass gain in FW II [g mol^{-1}]	Apparent mass loss in RV I [g mol^{-1}]
Salt	(anion + *n* solvent)	(anion + *n* solvent)
LiCl	215 ($n = 9.9$)	180 ($n = 8.0$)
NaCl	167 ($n = 7.3$)	169 ($n = 7.4$)
KCl	226 ($n = 10.5$)	212 ($n = 9.8$)
CsCl	176 ($n = 7.8$)	172 ($n = 7.6$)

transport of bulky anions across the polymer/electrolyte interface and significant, cumulative mass trapping after repeated redox cycling (Figure 4). These observations indicate that electrochemical devices containing bulky anions, such as the popular bistriflimide anion (which has the same ionic radius as tetraphenylborate[41]), should display subpar performance and/or electrochemical cycle stability if vapor deposited PEDOT films are used as the redox active layer.

3. Conclusion

Cyclic voltammetry and electrogravimetry measurements were conducted using an electrochemical quartz crystal microbalance to understand ion transport across a polymer/electrolyte interface in PEDOT films prepared by two widely used vapor deposition methods, oCVD and VPP. Though conductive films of the same chemical composition were obtained using these two different deposition methods, no similarities in electrochemical behavior and stability were observed. Our investigations revealed two main differences. First, little to no mass trapping with repeated doping/dedoping cycles was observed in PEDOT-oCVD, implying better stability to redox cycling, while PEDOT-VPP showed significant mass trapping after each electrochemical doping/dedoping cycle, even after two consecutive cycles. Second, permselectivity (the preferential motion of ions of one polarity, + or −, over the other) was observed in oCVD PEDOT as a generic behavior across different electrolytes. Such differences were attributed to the uniform distribution of nanometer-sized pores in oCVD PEDOT films, whereas VPP PEDOT films had rough surfaces and widely distributed micrometer to nanometer sized pores.

Currently, the electrical longevity and fatigue resistance of polymer-based supercapacitors pales in comparison to the tireless performance of porous carbon-based devices. This comparative instability is widely attributed to steadily increasing electrolyte ion trapping in the redox-active polymer layer upon repeated charging/discharging cycles.[44,45] Indeed, our results confirm that PEDOT films deposited using VPP display detrimental mass trapping with electrochemical cycling. Importantly, our results also indicate that changing the method of film deposition to oCVD creates films with comparatively minimal redox-associated mass trapping. This revelation is notable because, thus far, high conductivities in polymer films are primarily sought after, no matter the deposition condition, and little distinction has previously been made between VPP and oCVD. Our studies highlight that subtle differences between vapor deposition methods can have significant ramifications on the ultimate performance and longevity of charge storage devices.

Permselectivity is important for obtaining high on/off ratios and low threshold voltages in organic electrochemical transistors (OECTs). OECT-based ion sensors containing the composite material PEDOT:PSS typically also contain an ion-selective membrane (ISE),[15] though some reports claim that the PSS component can partially act as a cation-specific ISE at certain pH ranges.[46] For all other doped conducting polymers, permselectivity failure is highly likely[36] and, therefore, the anion permselectivity displayed by the oCVD PEDOT films studied herein is a powerful, unique characteristic.

Finally, we note that the electrogravimetric studies presented herein provide useful empirical information about the transport of ions across a polymer/electrolyte interface. Detailed information about ion transport within the vapor deposited PEDOT films can best be obtained using a different testing platform and sample device,[21,22] which will be the focus of future studies.

4. Experimental Section

General Considerations: All chemicals were purchased from Sigma-Aldrich and used without further purification. Scanning electron microscopy (SEM) was performed using a Magellan 400 field emission scanning electron microscope (FESEM). Conductivities were calculated from resistivity measurements made on films deposited on glass substrates using a home-built four-point probe test station. Film thicknesses were measured on a Veeco Dektak 150 profilometer.

Film Preparation: Films of *p*-doped PEDOT were directly deposited on a 5 MHz Au quartz crystal wrap-around electrode (Gamry) using either oxidative chemical vapor deposition (oCVD) or VPP. A contact mask was attached to the circumference of the crystal before polymer deposition to preserve uncoated gold contact pads for subsequent electrochemical measurements.

A previously described reaction chamber and process parameters[40–42] were used to create the PEDOT films via oCVD (Figure 1). Iron (III) chloride was used as the oxidant and 3,4-ethylenedioxythiophene (EDOT) was used as the monomer. The total pressure in the chamber was maintained at 100 mTorr and the substrate stage temperature was maintained at 120 °C during deposition. oCVD was performed for 20 min, at an effective film forming rate of 0.5–0.8 Å s^{-1}.

For films obtained via VPP (Figure 1), a quartz crystal electrode was, first, dropcast with 0.25 M aqueous $FeCl_3$ solution, placed on a hot plate and annealed at 120 °C under inert atmosphere. Next, a shallow container with EDOT was placed adjacent to the oxidant-coated electrode, and the two components were covered with a large inverted crystallization dish (to create a closed environment) and heated to 120 °C for 30 min.

Both oCVD PEDOT and VPP PEDOT films were rinsed with copious amounts of methanol and subsequently immersed in 5 mL of methanol for 30 min to effect complete removal of $FeCl_3$ and other reaction byproducts, as previously established.[47] The films were finally vacuum dried for 1 h at room temperature before electrochemical and electrogravimetric measurements were performed.

As previously described,[40,41] films obtained using both oCVD and VPP were slightly *p*-doped because of the availability of excess oxidant during deposition and remained *p*-doped even after rinsing/drying. Because of the iron (III) chloride oxidant used, chloride counterions were present in the as-deposited films.[41]

The thickness of the PEDOT films was measured after rinsing/drying. Films obtained using oCVD were consistently 80 nm thick.

 © 2017 WILEY-VCH Verlag GmbH & Co. KGaA, Weinheim

Films obtained using VPP were of highly variable thickness, depending on the batch; quartz sensors coated with 100 nm thick PEDOT films were identified and used for the electrochemical studies performed herein. Conductivities of the PEDOT-VPP and PEDOT-oCVD films were measured using films deposited on glass substrates following the previously described deposition procedures. The measured conductivities of five different PEDOT-oCVD films were 210 S cm^{-1} and those of PEDOT-VPP films varied between 190 and 270 S cm^{-1}, depending on the batch.

Electrochemical-Electrogravimetric Measurements: Simultaneous cyclic voltammetry and electrogravimetric measurements were carried out using a Gamry Interface 1000B potentiostat equipped with an electrochemical quartz crystal microbalance (eQCM-10 M measurement cell). All electrochemical characterization experiments were carried out using a three-electrode setup, with a platinum wire counter electrode and an aqueous Ag/AgCl reference electrode. Gold quartz crystal sensors (5 MHz Au Quartz Crystal Wrap-Around electrode from Gamry Instruments) coated with different *p*-doped PEDOT films (as described above) were used as a combined working electrode and gravimetric sensor. All electrolytes used in this work were of 0.5 M concentration, except for sodium tetraphenylborate, which was 0.2 M in H_2O: ethanol (2:1).

To perform the measurement, the three electrodes were fitted into preassigned slots in the eQCM-10 M cell and electrolyte was then added to the cell. As soon as the PEDOT-coated working electrode was contacted with the electrolyte, solvent and/or ion diffusion into/out of the PEDOT film was observed in the gravimetric sensing channel, even in the absence of an applied potential (Figure S1, Supporting Information). On average, 0.5 µg of increased mass was observed over 20 min for all electrodes studied herein. Therefore, the assembled eQCM cell (three electrodes and electrolyte) was allowed to rest for 20 min and achieve mass equilibrium before staring a CV-EG scan. Scan rates for all measurements were 10 mV s^{-1}.

eQCM measurements rely on a thin piezoelectric quartz crystal sandwiched between two metal electrodes.[33] An alternating electric field is applied across the two metal electrodes, which causes the crystal to vibrate at its resonance frequency. The resonance frequency is sensitive to the mass of the crystal. If a thin coating is applied directly onto its surface, then mass changes in this coating will be transduced by the quartz crystal as a shift in its resonance frequency, assuming no acoustic losses within the coating and at the coating/crystal interface. The frequency shift, Δf, can then be converted to a mass change, Δm, using the Sauerbrey equation

$$\Delta m = -\Delta f \cdot \frac{\sqrt{\rho_q \cdot \mu_q}}{2 f_n} = -C_f \cdot \Delta f \quad (3)$$

Here ρ_q is the density of quartz, μ_q is the shear modulus of quartz, f_0 is the fundamental resonance frequency of the quartz, and C_f is a sensitivity factor.

Previously reported eQCM studies on electrodeposited conjugated polymer films[35–37] confirm that 100 nm thick coatings of conducting polymers on a quartz crystal sensor do not display notable acoustic losses/modulation within the film or at the polymer/crystal interface. Therefore, it can be reasonably assume that any frequency shifts recorded by the PEDOT-coated quartz crystals studied herein are a direct measure of mass changes in the PEDOT layer.

Supporting Information

Supporting Information is available from the Wiley Online Library or from the author.

Acknowledgements

The authors gratefully acknowledge financial support from the US Air Force Office of Scientific Research, under Agreement No. FA9550-14-1-0128. T.L.A. also gratefully acknowledges partial support by the David and Lucille Packard Foundation.

Conflict of Interest

The authors declare no conflict of interest.

Keywords

conducting polymers, electrochemistry, electrogravimetry, ion transport, vapor coatings

Received: July 20, 2017
Revised: August 11, 2017
Published online:

[1] Y. Guo, M. T. Otley, M. Li, X. Zhang, S. K. Sinha, G. M. Treich, G. A. Sotzing, *ACS Appl. Mater. Interfaces* **2016**, *8*, 26998.
[2] a) S. Takamatsu, T. Takahata, M. Muraki, E. Iwase, K. Matsumoto, I. Shimoyama, *J. Micromech. Microeng.* **2010**, *20*, 075017; b) S. Sekine, Y. Ido, T. Miyake, K. Nagamine, M. Nishizawa, *J. Am. Chem. Soc.* **2010**, *132*, 13174; c) Y. Kim, J. Na, C. Park, H. Shin, E. Kim, *ACS Appl. Mater. Interfaces* **2015**, *7*, 16279.
[3] J. F. Mike, J. L. Lutkenhaus, *J. Polym. Sci., Part B: Polym. Phys.* **2013**, *51*, 468.
[4] J. F. Mike, J. L. Lutkenhaus, *ACS Macro Lett.* **2013**, *2*, 839.
[5] J. A. Lee, M. K. Shin, S. H. Kim, H. U. Cho, G. M. Spinks, G. G. Wallace, M. D. Lima, X. Lepro, M. E. Kozlov, R. H. Baughman, S. J. Kim, *Nat. Commun.* **2013**, *4*, 1970.
[6] M. Zhu, Y. Huang, Y. Huang, H. Li, Z. Wang, Z. Pei, Q. Xue, H. Geng, C. Zhi, *Adv. Mater.* **2017**, *29*, 1605137.
[7] A. Liu, P. Kovacik, N. Peard, W. Tian, H. Goktas, J. Lau, B. Dunn, K. K. Gleason, *Adv. Mater.* **2017**, *29*, 1606091.
[8] D. Khodagholy, T. Doublet, P. Quilichini, M. Gurfinkel, P. Leleux, A. Ghestem, E. Ismailova, T. Hervé, S. Sanaur, C. Bernard, G. G. Malliaras, *Nat. Commun.* **2013**, *4*, 1575.
[9] L. K. Povlich, K. E. Feldman, B. Wei, T. Eom, B. S. Shim, D. C. Martin, *Comprehensive Biomaterials II*, Elsevier, Oxford **2017**, p. 664.
[10] D. C. Martin, *MRS Commun.* **2015**, *5*, 131.
[11] S. Kumar, S. Kumar, C. M. Pandey, B. D. Malhotra, *J. Phys.: Conf. Ser.* **2016**, *704*, 012010.
[12] L. Ouyang, C. L. Shaw, C. C. Kuo, A. L. Griffin, D. C. Martin, *J. Neural Eng.* **2014**, *11*, 026005.
[13] D. Khodagholy, T. Doublet, M. Gurfinkel, P. Quilichini, E. Ismailova, P. Leleux, T. Herve, S. Sanaur, C. Bernard, G. G. Malliaras, *Adv. Mater.* **2011**, *23*, 268.
[14] S. Y. Yang, F. Cicoira, R. Byrne, F. Benito-Lopez, D. Diamond, R. M. Owens, G. G. Malliaras, *Chem. Commun.* **2010**, *46*, 7972.
[15] M. Sessolo, J. Rivnay, E. Bandiello, G. G. Malliaras, H. J. Bolink, *Adv. Mater.* **2014**, *26*, 4803.
[16] Y. van de Burgt, E. Lubberman, E. J. Fuller, S. T. Keene, G. C. Faria, S. Agarwal, M. J. Marinella, A. Alec Talin, A. Salleo, *Nat. Mater.* **2017**, *16*, 414.
[17] N. B. Teran, J. R. Reynolds, *Chem. Mater.* **2017**, *29*, 1290.
[18] a) K. Cao, D. E. Shen, A. M. Österholm, J. A. Kerszulis, J. R. Reynolds, *Macromolecules* **2016**, *49*, 8498; b) A. M. Österholm, D. E. Shen, D. S. Gottfried, J. R. Reynolds, *Adv. Mater. Technol.* **2016**, *1*, 1600063.

 © 2017 WILEY-VCH Verlag GmbH & Co. KGaA, Weinheim

[19] A. Maziz, A. Concas, A. Khaldi, J. Stålhand, N.-K. Persson, E. W. H. Jager, *Sci. Adv.* **2017**, *3*, e1600327.
[20] J. Rivnay, S. Inal, B. A. Collins, M. Sessolo, E. Stavrinidou, X. Strakosas, C. Tassone, D. M. Delongchamp, G. G. Malliaras, *Nat. Commun.* **2016**, *7*, 11287.
[21] X. Wang, B. Shapiro, E. Smela, *Adv. Mater.* **2004**, *16*, 1605.
[22] X. Wang, E. Smela, *J. Phys. Chem. C* **2009**, *113*, 369.
[23] S. E. Atanasov, M. D. Losego, B. Gong, E. Sachet, J.-P. Maria, P. S. Williams, G. N. Parsons, *Chem. Mater.* **2014**, *26*, 3471.
[24] B. Yao, H. Wang, Q. Zhou, M. Wu, M. Zhang, C. Li, G. Shi, *Adv. Mater.* **2017**, *29*, 1700974.
[25] O. Bubnova, Z. U. Khan, H. Wang, S. Braun, D. R. Evans, M. Fabretto, P. Hojati-Talemi, D. Dagnelund, J.-B. Arlin, Y. H. Geerts, S. Desbief, D. W. Breiby, J. W. Andreasen, R. Lazzaroni, W. M. Chen, I. Zozoulenko, M. Fahlman, P. J. Murphy, M. Berggren, X. Crispin, *Nat. Mater.* **2014**, *13*, 190.
[26] A. Elschner, S. Kirchmeyer, W. Lovenich, U. Merker, K. Reuter, *PEDOT: Principles and Applications of an Intrinsically Conductive Polymer*, CRC Press, Boca Raton, FL **2011**.
[27] H. Shi, C. Liu, Q. Jiang, J. Xu, *Adv. Electron. Mater.* **2015**, *1*, 1500017.
[28] J. M. Leger, *Adv. Mater.* **2008**, *20*, 837.
[29] G. Tarabella, F. M. Mahvash, N. Coppede, F. Barbero, S. Iannotta, C. Santato, F. Cicoira, *Chem. Sci.* **2013**, *4*, 1395.
[30] M. D. Levi, G. Salitra, N. Levy, D. Aurbach, J. Maier, *Nat. Mater.* **2009**, *8*, 872.
[31] J. M. Griffin, A. C. Forse, W.-Y. Tsai, P.-L. Taberna, P. Simon, C. P. Grey, *Nat. Mater.* **2015**, *14*, 812.
[32] M. D. Levi, N. Levy, S. Sigalov, G. Salitra, D. Aurbach, J. Maier, *J. Am. Chem. Soc.* **2010**, *132*, 13220.
[33] W. Y. Tsai, P. L. Taberna, P. Simon, *J. Am. Chem. Soc.* **2014**, *136*, 8722.
[34] A. C. Forse, C. Merlet, J. M. Griffin, C. P. Grey, *J. Am. Chem. Soc.* **2016**, *138*, 5731.
[35] A. R. Hillman, S. J. Daisley, S. Bruckenstein, *Electrochem. Commun.* **2007**, *9*, 1316.
[36] A. R. Hillman, S. J. Daisley, S. Bruckenstein, *Electrochim. Acta* **2008**, *53*, 3763.
[37] A. R. Hillman, S. J. Daisley, S. Bruckenstein, *Phys. Chem. Chem. Phys.* **2007**, *9*, 2379.
[38] L. Allison, S. Hoxie, T. L. Andrew, *Chem. Commun.* **2017**, *53*, 7182.
[39] L. Yuan, B. Yao, B. Hu, K. Huo, W. Chen, J. Zhou, *Energy Environ. Sci.* **2013**, *6*, 470.
[40] L. Zhang, M. Fairbanks, T. L. Andrew, *Adv. Funct. Mater.* **2017**, *27*, 1700415.
[41] N. Cheng, L. Zhang, J. J. Kim, T. L. Andrew, *J. Mater. Chem. C* **2017**, *5*, 5787.
[42] A. M. Coclite, R. M. Howden, D. C. Borrelli, C. D. Petruczok, R. Yang, J. L. Yague, A. Ugur, N. Chen, S. Lee, W. J. Jo, A. Liu, X. Wang, K. K. Gleason, *Adv. Mater.* **2013**, *25*, 5392.
[43] I. Shown, A. Ganguly, L.-C. Chen, K.-H. Chen, *Energy Sci. Eng.* **2015**, *3*, 2.
[44] J. Kim, J. Lee, J. You, M.-S. Park, M. S. A. Hossain, Y. Yamauchi, J. H. Kim, *Mater. Horiz.* **2016**, *3*, 517.
[45] S. Kazemiabnavi, Z. Zhang, K. Thornton, S. Banerjee, *J. Phys. Chem. B* **2016**, *120*, 5691.
[46] P. Lin, F. Yan, H. L. W. Chan, *ACS Appl. Mater. Interfaces* **2010**, *2*, 1637.
[47] S. G. Im, K. K. Gleason, *Appl. Phys. Lett.* **2007**, *90*, 152112.

 © 2017 WILEY-VCH Verlag GmbH & Co. KGaA, Weinheim